



Figures and figure supplements

Molecular mechanism of activation-triggered subunit exchange in Ca²⁺/calmodulin-dependent protein kinase II

Moitrayee Bhattacharyya *et al*

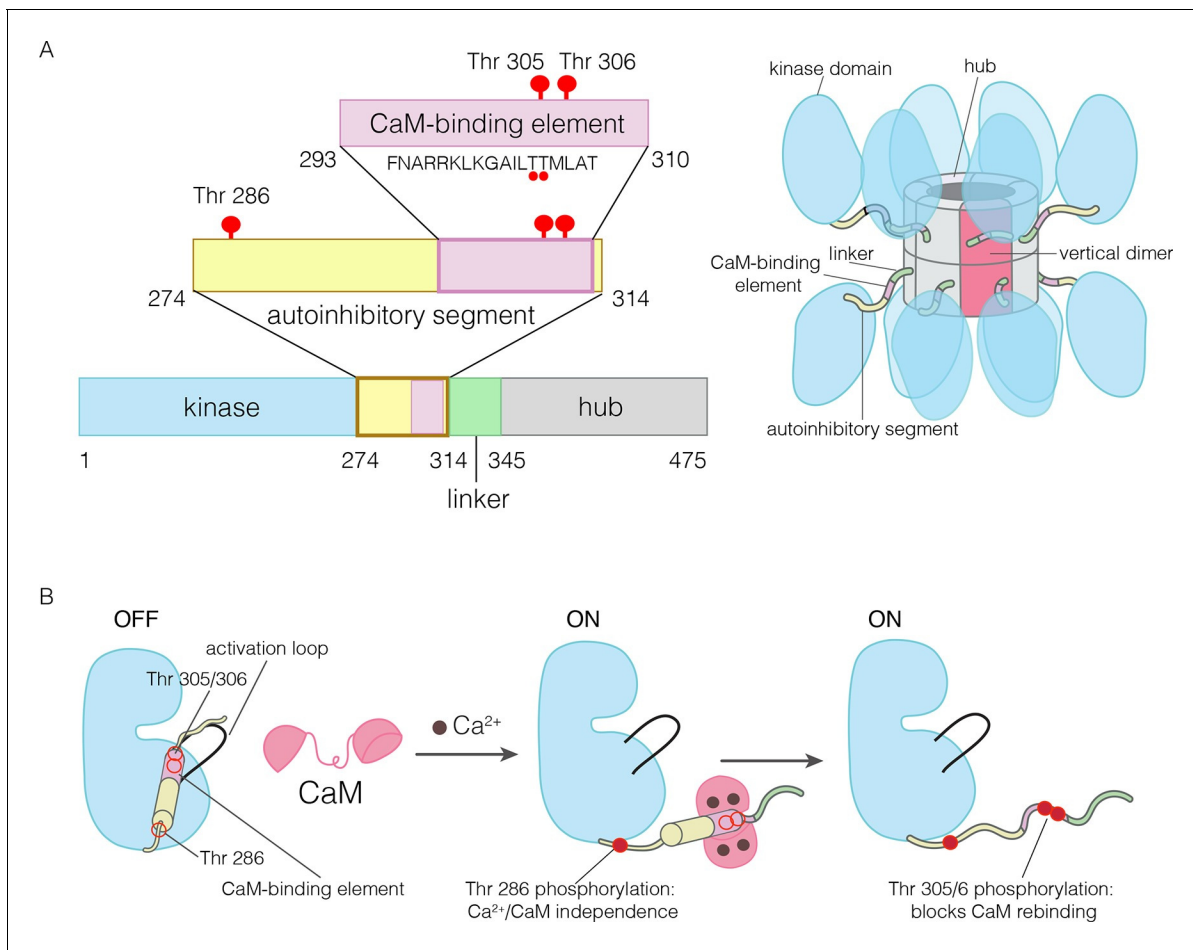


Figure 1. The domains of human CaMKII- α . **(A)** The architecture of the CaMKII holoenzyme is shown on the right. The hub domain forms a dodecamer or tetradecamer, and the kinase domains are flexibly linked to it by the autoinhibitory segment. **(B)** The autoinhibitory segment contains three critical sites of phosphorylation: Thr 286, Thr 305 and Thr 306. Activation by Ca²⁺/CaM results in phosphorylation at Thr 286, which renders the enzyme independent of Ca²⁺/CaM. Further phosphorylation of Thr 305 and Thr 306 prevents re-binding of Ca²⁺/CaM.

DOI: [10.7554/eLife.13405.003](https://doi.org/10.7554/eLife.13405.003)

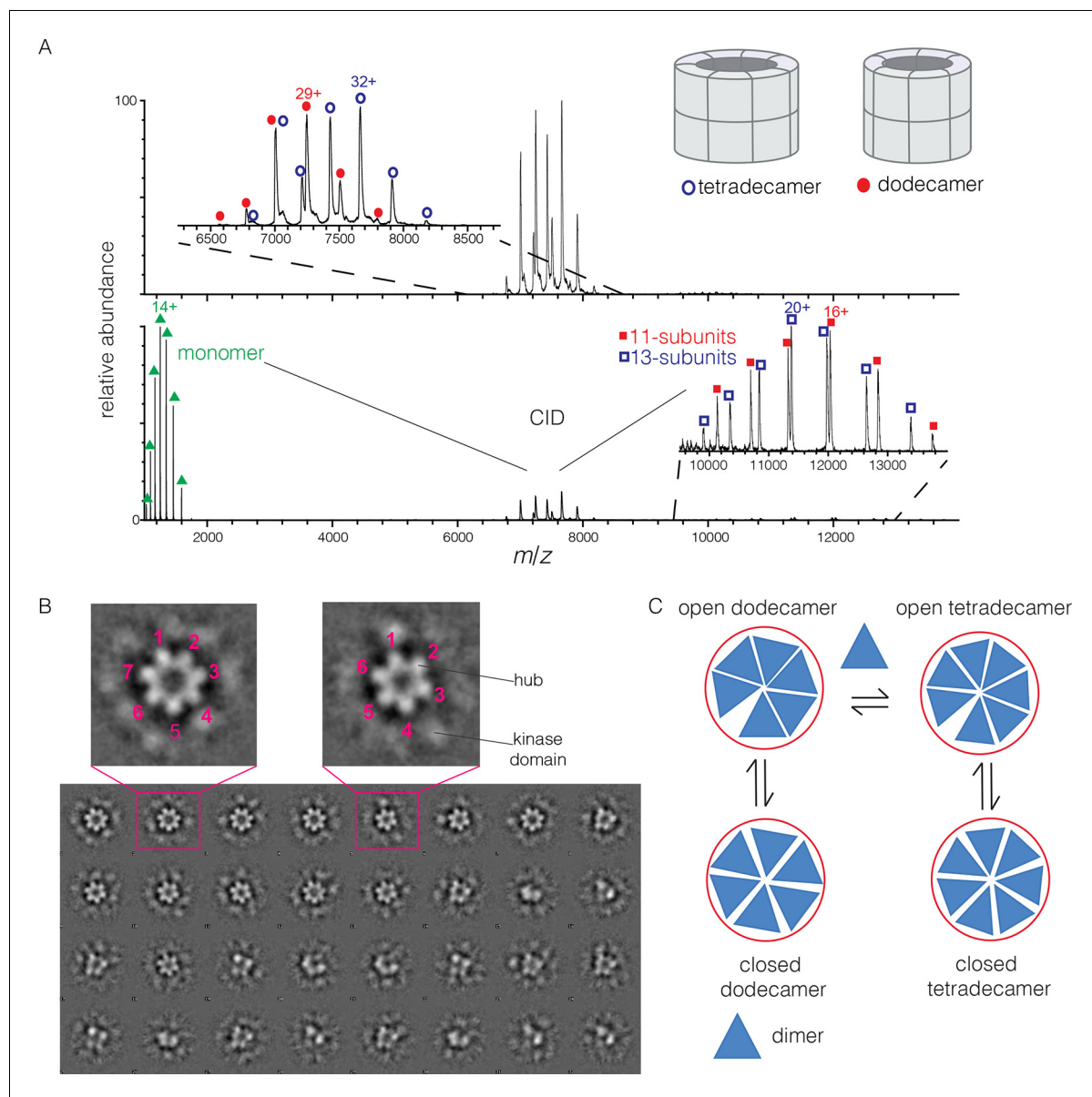


Figure 2. Human CaMKII- α forms both dodecamers and tetradecamers. (A) Native ESI-MS spectra of the human CaMKII- α hub reveals a ~1:1 mixture of dodecamers and tetradecamers (top panel). Collision-induced dissociation (CID) MS/MS of hub parent ions shows the presence of fragment ions corresponding to a highly charged hub monomer and a mixture of 11-subunit and 13-subunit species, clearly showing the mixed stoichiometry of the parent ion (bottom panel). (B) Two-dimensional class averages of images from negative-stain electron microscopy for human CaMKII- α show the existence of holoenzyme particles with both six-fold and seven fold symmetry. A subset of 32 of the 50 total class averages is shown, and an expanded view of two class averages is shown, one with seven-fold and one with six-fold symmetry. (C) A possible pathway for the transition between the dodecameric and tetradecameric species through the addition or loss of a dimer unit.

DOI: [10.7554/eLife.13405.004](https://doi.org/10.7554/eLife.13405.004)

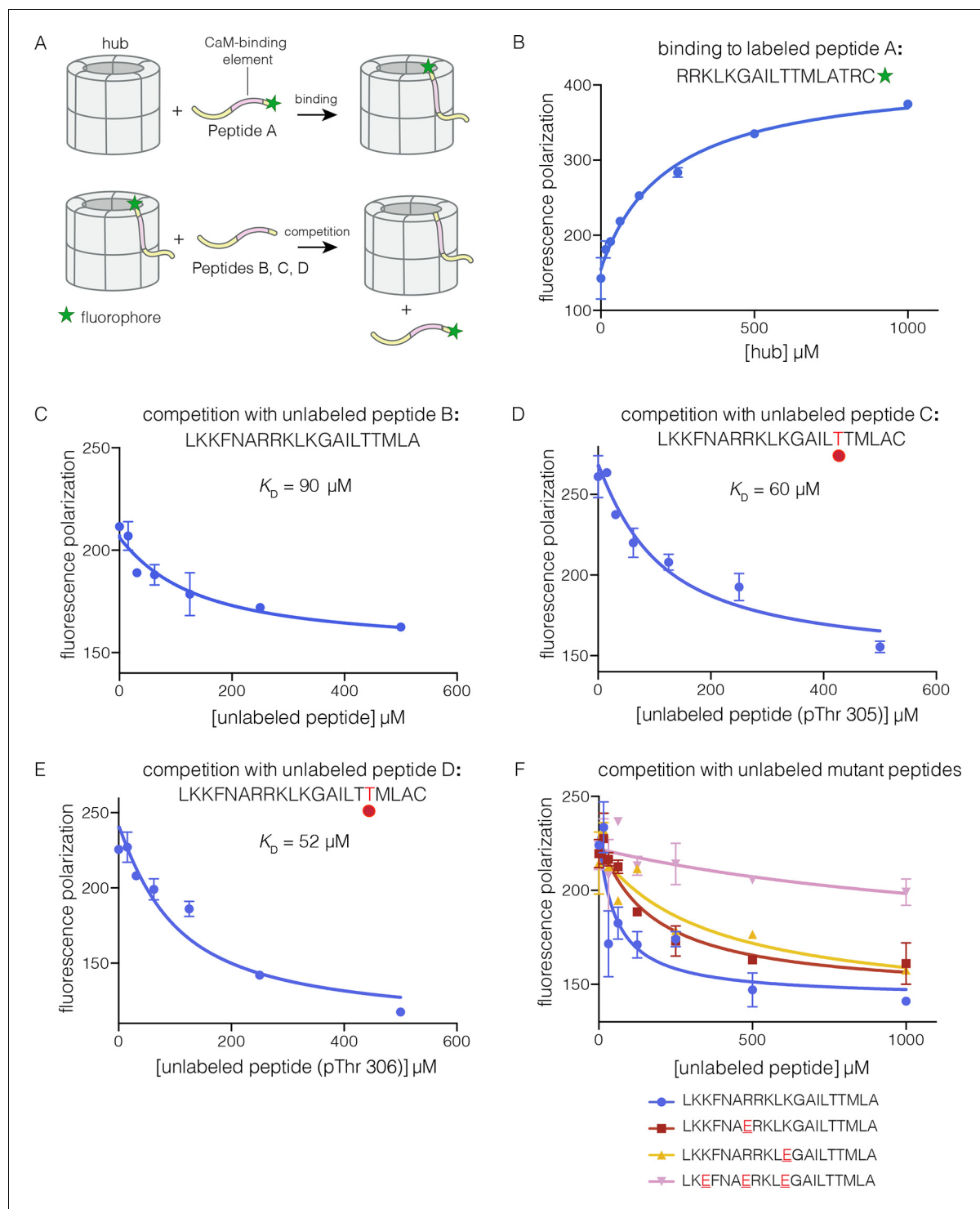


Figure 3. Binding of the CaM-binding element to the human CaMKII- α hub. (A) Schematic diagram of the binding experiments. (B) Direct titration of the hub to the labeled peptide A. Fluorescence polarization of the labeled peptide increases as a function of total hub concentration. The value of K_D derived from these data is $\sim 100 \mu\text{M}$, but due to evidence for non-saturable binding, we relied instead on competition experiments to obtain K_D values. (C–E) Competition experiments with unlabeled peptides. Addition of labeled peptide is followed by competition with excess unlabeled peptide of the same sequence (except for the competition with peptide B, where labeled Peptide A was used for initial binding). (F) Competition with mutant peptides. The hub is bound to labeled peptide A and fluorescence polarization is measured as a function of the total concentration of unlabeled mutant peptides. The sites of mutation in these peptides are highlighted in red and underlined. Fluorescence polarization is a ratio involving light intensities that are parallel and perpendicular to the plane of linearly polarized excitation light and is therefore reported as a dimensionless number. *Figure 3 continued on next page*

Figure 3 continued

DOI: [10.7554/eLife.13405.005](https://doi.org/10.7554/eLife.13405.005)

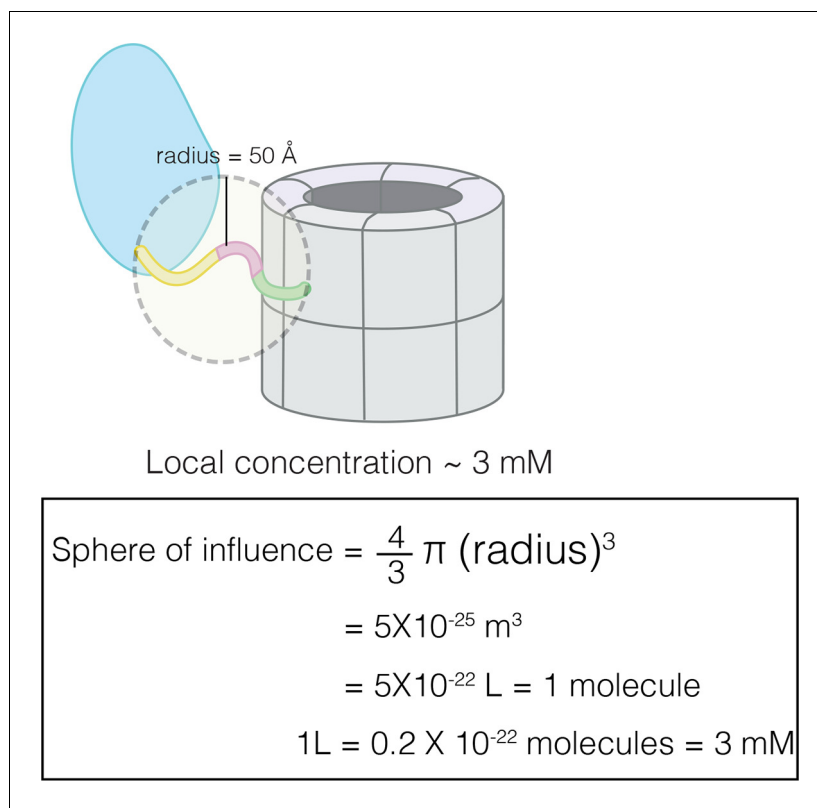


Figure 3—figure supplement 1. Calculation of effective concentration of the CaM-binding element by assuming that the linker restricts it to within 50 Å of the hub. This corresponds to an effective concentration of ~3 mM.

DOI: [10.7554/eLife.13405.006](https://doi.org/10.7554/eLife.13405.006)

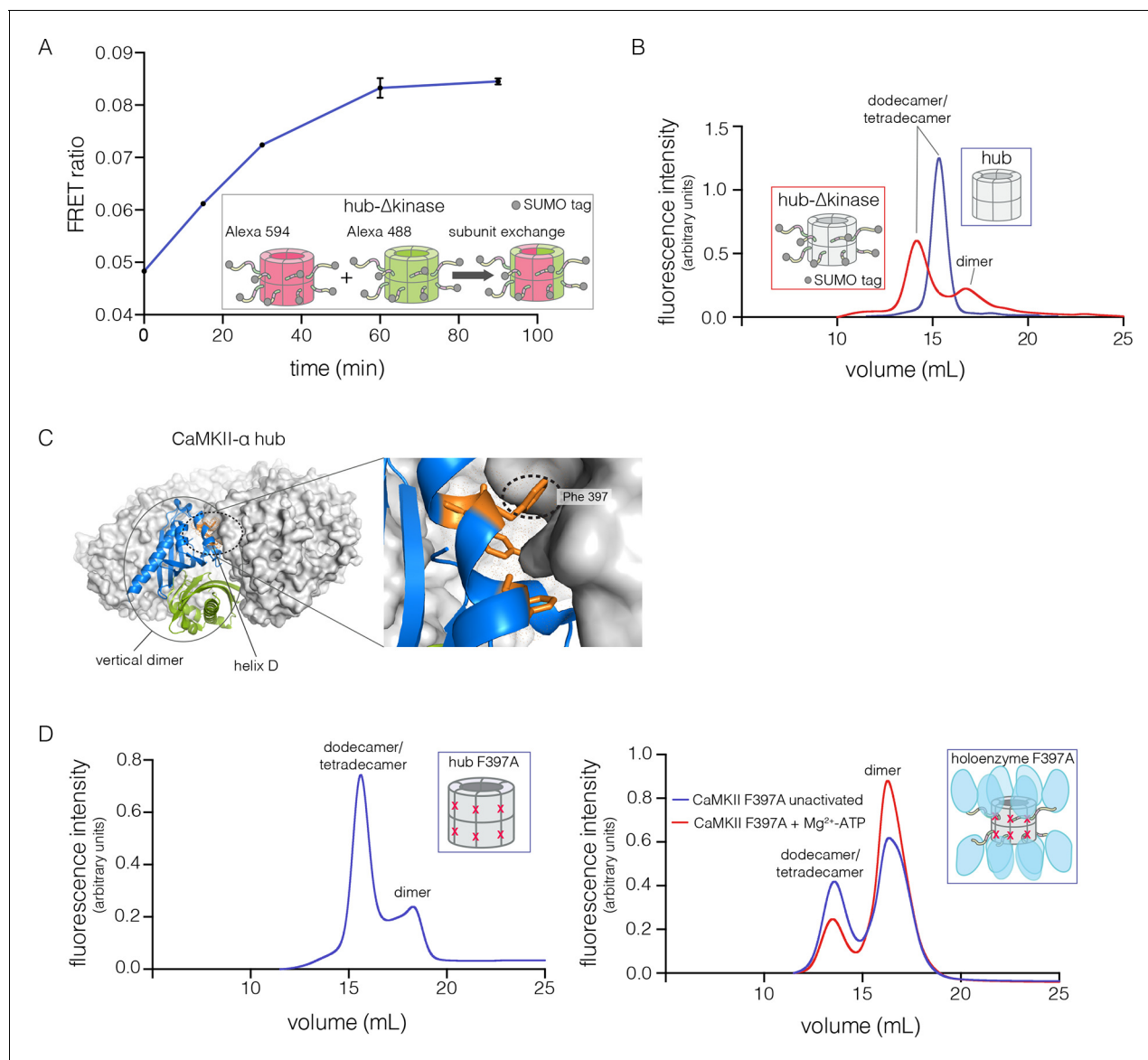


Figure 4. Analysis of kinase domain deletion and hub mutation. **(A)** Spontaneous subunit exchange in CaMKII lacking only the kinase domain (hub- Δ kinase). Increase in the FRET-ratio (see Materials and methods) is graphed as a function of time for the hub- Δ kinase construct (also see **Figure 4—figure supplement 1**). The increase in FRET upon mixing donor and acceptor-labeled proteins is indicative of subunit exchange (**Stratton et al., 2014**). **(B)** Analytical gel filtration of isolated hub domains and hub- Δ kinase from human CaMKII- α . The isolated hub shows one peak, with a retention volume corresponding to dodecamer/tetradecamer, as estimated from calibration data (see **Figure 4—figure supplement 4**). The hub- Δ kinase construct shows two peaks, corresponding to dodecamer/tetradecamer and dimer, respectively. Note that the hub- Δ kinase construct includes a SUMO tag, which accounts for its smaller retention volume compared to that for the hub alone. The gel filtration traces are normalized so that they have the same area under the curve. **(C)** A view of the lateral interface between subunits in adjacent vertical dimers of CaMKII- α (PDB code: 1HKX). **(D)** Replacement of Phe 397 at the hub interface by alanine leads to release of dimers from the isolated hub (left) and the holoenzyme (right). Pre-incubation of F397A holoenzyme with Mg²⁺-ATP enhances the amount of dimers released, which is correlated with phosphorylation of Thr 305 and Thr 306 (data not shown). See also mass spectrometric analysis of the F397A mutant hub (**Figure 4—figure supplement 3**).

DOI: [10.7554/eLife.13405.007](https://doi.org/10.7554/eLife.13405.007)

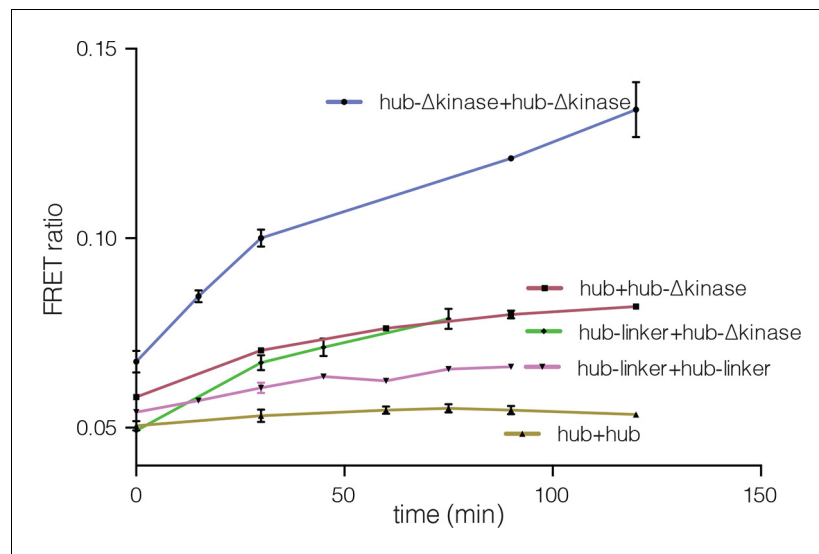


Figure 4—figure supplement 1. Subunit exchange between various truncation constructs of CaMKII lacking the kinase domain (hub-Δkinase), the kinase domain and the autoinhibitory segment (hub-linker) and the hub alone. Increase in the FRET-ratio (see Materials and methods) is graphed as a function of time. The increase in FRET upon mixing donor and acceptor-labeled proteins is indicative of subunit exchange (Stratton et al., 2014). The variability in the FRET ratio between experiments is due to differences in the percentage of labeled cysteine residues and fluorophore environments in different protein preparations.

DOI: [10.7554/eLife.13405.008](https://doi.org/10.7554/eLife.13405.008)

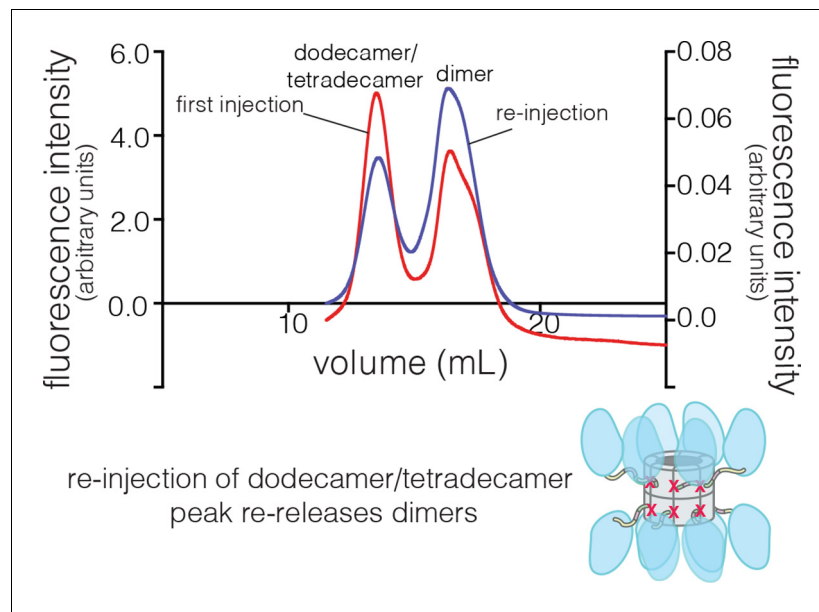


Figure 4—figure supplement 2. Collection and re-injection of the dodecameric/tetradecameric peak for the human CaMKII- α F397A mutant re-releases dimers. The fluorescence intensity for the first injection is shown on the left y-axis and that for the re-injection of the dodecamer/tetradecamer peak is shown on the right y-axis.
[DOI: 10.7554/eLife.13405.009](https://doi.org/10.7554/eLife.13405.009)

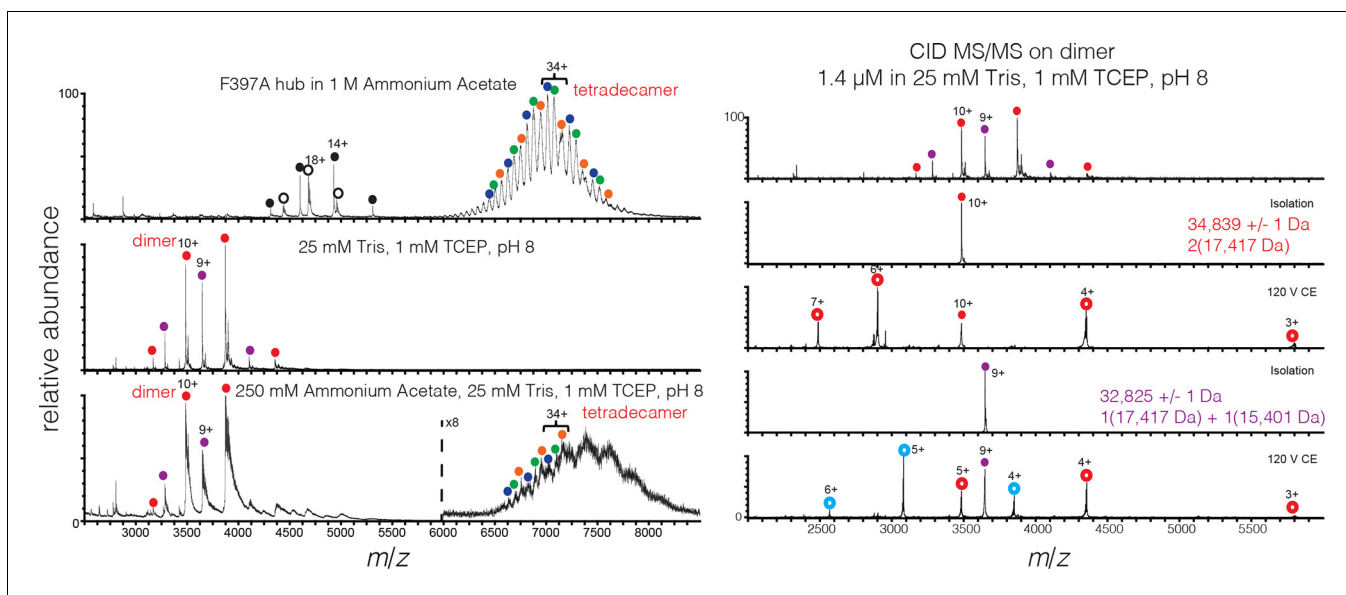


Figure 4—figure supplement 3. Mass spectra of 200 μM mutant hub in 1 M ammonium acetate (top), and 2 μM mutant hub in 25 mM Tris, 1 mM TCEP, pH 8 (middle) and 250 mM ammonium acetate, 25 mM Tris, 1 mM TCEP, pH 8 (bottom). Heterogeneity is observed in the dimer and tetradecamer species due to incomplete cleavage of the His tag from the monomer. The measured mass of each species was: dimer (red) $34,839 \pm 1$ Da, dimer-1 His tag (purple) $32,825 \pm 1$ Da, tetradecamer-1 His tag (orange) 242120 ± 78 Da, tetradecamer-2 His tags (green) 240104 ± 16 Da, and tetradecamer-3 His tags (blue) 238048 ± 23 Da. Oligomer identity was confirmed by CID (right panel).

DOI: [10.7554/eLife.13405.010](https://doi.org/10.7554/eLife.13405.010)

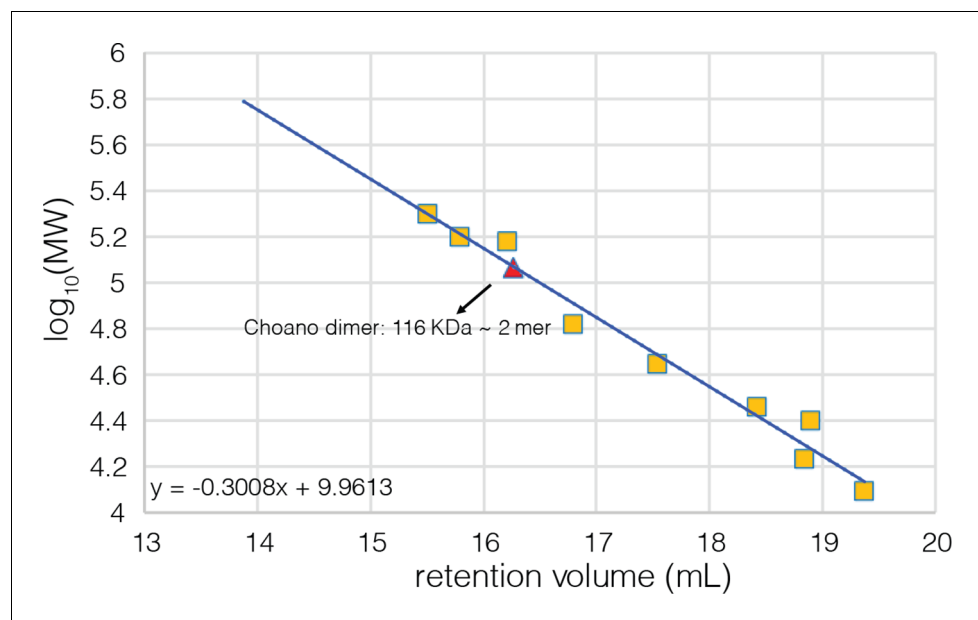


Figure 4—figure supplement 4. Calibration curve for the analytical gel filtration column. Beta amylase (200 kDa), gamma globulin (158 kDa), alcohol dehydrogenase (150 kDa), bovine serum albumin (66 kDa), chicken ovalbumin (44 kDa), carbonic anhydrase (29 kDa), gamma phosphatase (25 kDa), myoglobin (17 kDa), and cytochrome C (12.4 kDa) were used as molecular weight standards to calibrate the column and their retention volumes are indicated by yellow squares. The fitting equation is also shown on the plot.

DOI: [10.7554/eLife.13405.011](https://doi.org/10.7554/eLife.13405.011)

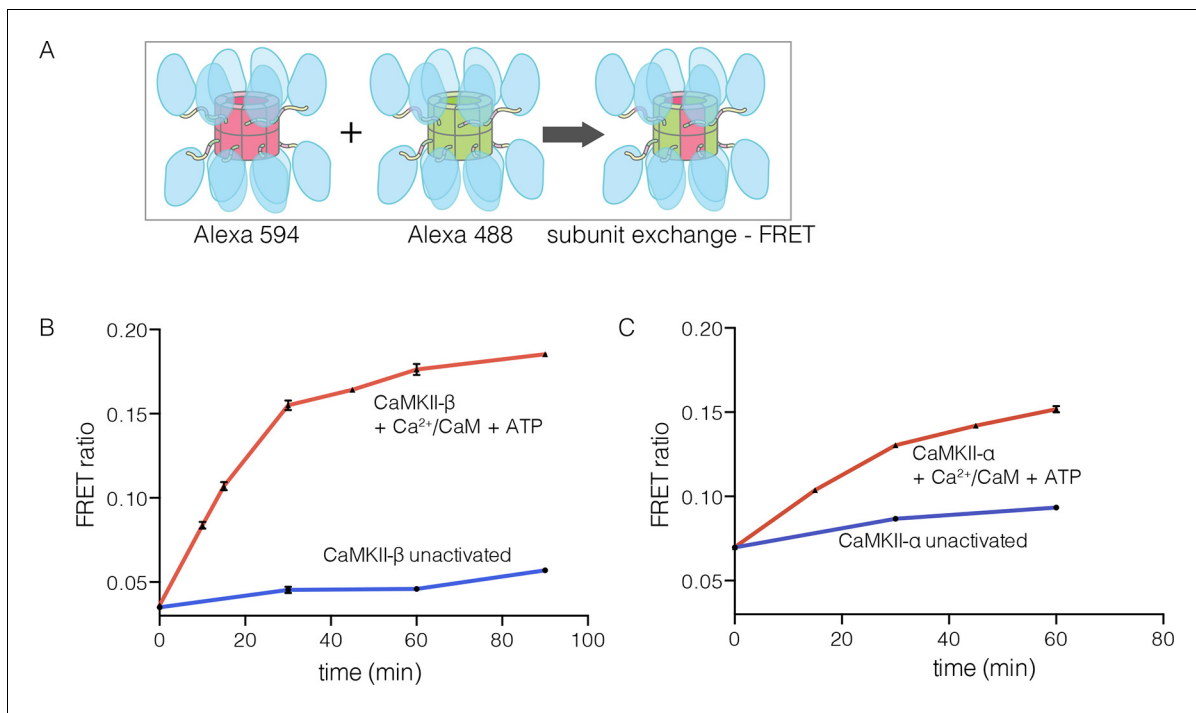


Figure 5. Subunit exchange in CaMKII- β . (A) Schematic diagram illustrating the design of solution FRET experiments for monitoring subunit exchange in CaMKII (Stratton *et al.*, 2014). (B, C) FRET ratio as a function of time for human CaMKII- β and human CaMKII- α . The difference in the extent of FRET between the experiments shown in Panels B and C is due to differences in the percentage of labeled cysteine residues and the fluorophore environments in different proteins.

DOI: [10.7554/eLife.13405.012](https://doi.org/10.7554/eLife.13405.012)

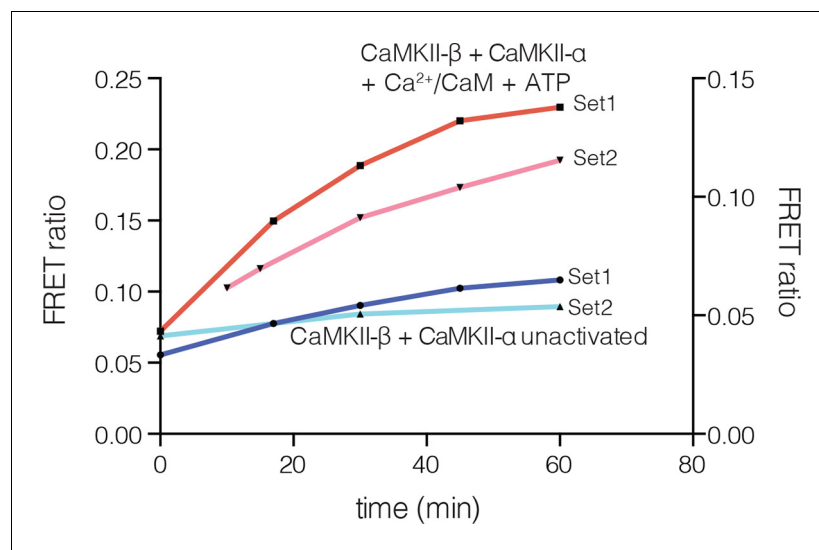


Figure 5—figure supplement 1. Subunit exchange between human CaMKII- β and CaMKII- α . FRET ratio as a function of time is graphed. The replicate data are shown on two different y-axes (set1 on left and set2 on right y-axis) due to the large differences in the absolute values of FRET ratio from the two different protein preparations used for this analysis.

DOI: [10.7554/eLife.13405.013](https://doi.org/10.7554/eLife.13405.013)

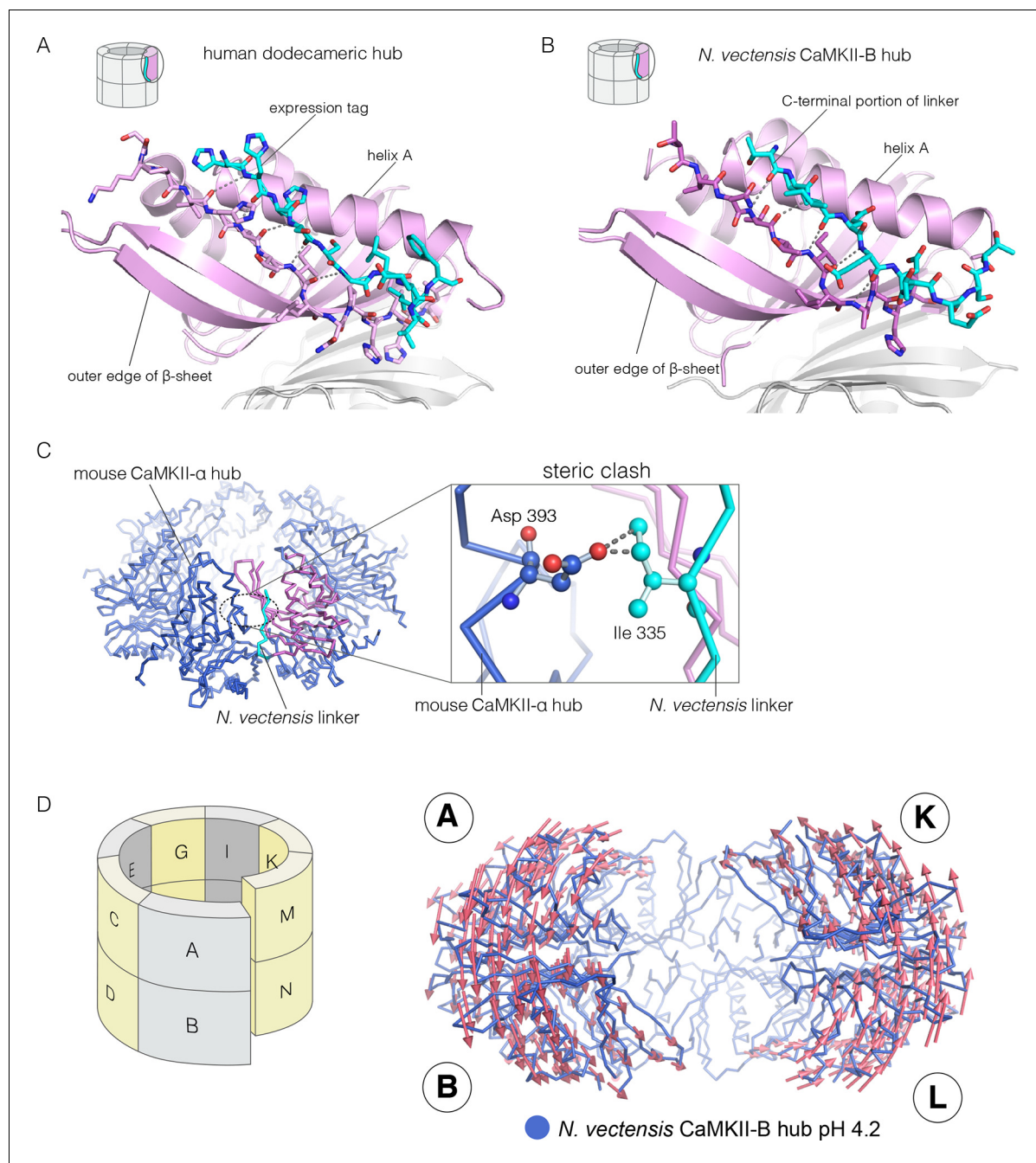


Figure 6. Docking of peptide segments onto the central β -sheet of the hub domain. (A) The N-terminal expression tag in human CaMKII- α docked on the open β -strand of the central β -sheet within the same hub subunit. (B) Linker residues in *N. vectensis* CaMKII-B hub (at pH 4.2) docked on the β -sheet of the hub subunit. (C) One subunit of the *N. vectensis* CaMKII-B hub, including the docked linker segment, is superimposed on the tetradecameric mouse CaMKII- α hub (PDB code: 1HKX). The *N. vectensis* hub domain is in magenta with the docked linker shown in cyan, and the CaMKII- α hub is in blue. The expanded view shows that the sidechain of Ile 335 in the linker of *N. vectensis* CaMKII-B hub collides with Asp 393 from helix D in the adjacent subunit of the mouse tetradecameric hub. (D) The distortion in the structure of *N. vectensis* CaMKII-B hub at pH 4.2. The spiral arrangement of the subunits is shown in the schematic diagram on the left, with each subunit labeled. The deviation between the closed-ring structure of *N. vectensis* CaMKII-A (pH 7.0) and the spiral form of the *N. vectensis* CaMKII-B structure is illustrated on the right, with the two structures aligned using subunits E, F, G and H. Arrows indicate displacement of the $\text{C}\alpha$ atoms in going from the closed-ring CaMKII-A hub structure to the opened-ring CaMKII-B hub. Each arrow is scaled by a factor of 2 and arrows are only shown for $\text{C}\alpha$ displacements greater than or equal to 2 Å. The structure shown is that of *N. vectensis* CaMKII-B hub. The M and N subunits are not shown for clarity.

DOI: 10.7554/eLife.13405.014

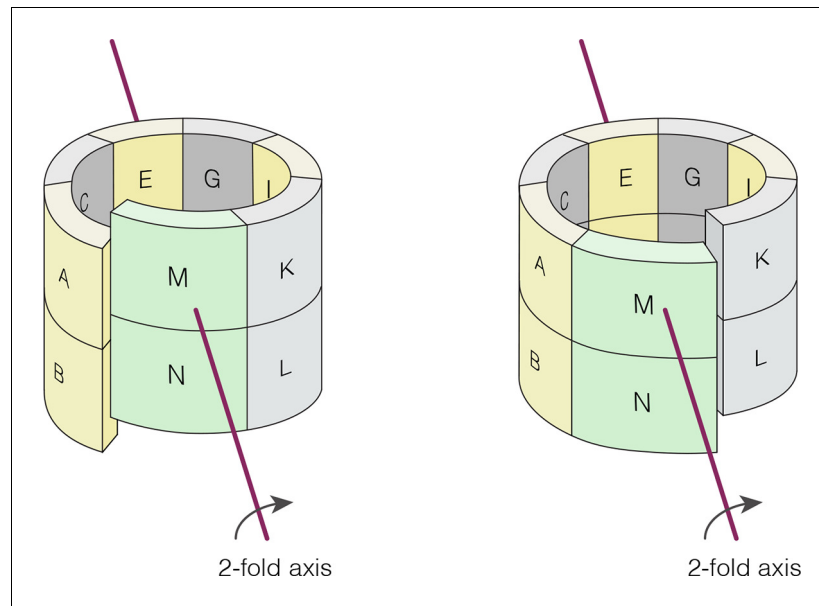


Figure 6—figure supplement 1. Crystallographic axis of two-fold symmetry runs through the middle of the tetramer formed by the E-F and G-H dimers in *N. vectensis* pH 4.2 structure (CaMKII-B hub). The left-handed “lock-washer” architecture allows 12 of the 14 subunits in the pH 4.2 structure to obey this axis of symmetry. The M-N dimer cannot obey the symmetry, because of the spiral geometry. The symmetry axis generates two copies of the M-N dimer. One copy is “joined” to the A-B dimer, and dislocated from the K-L dimer. The other copy is “joined” to the K-L dimer, but dislocated from the A-B dimer (see [Supplementary files 2 and 3](#)).

DOI: [10.7554/eLife.13405.015](https://doi.org/10.7554/eLife.13405.015)

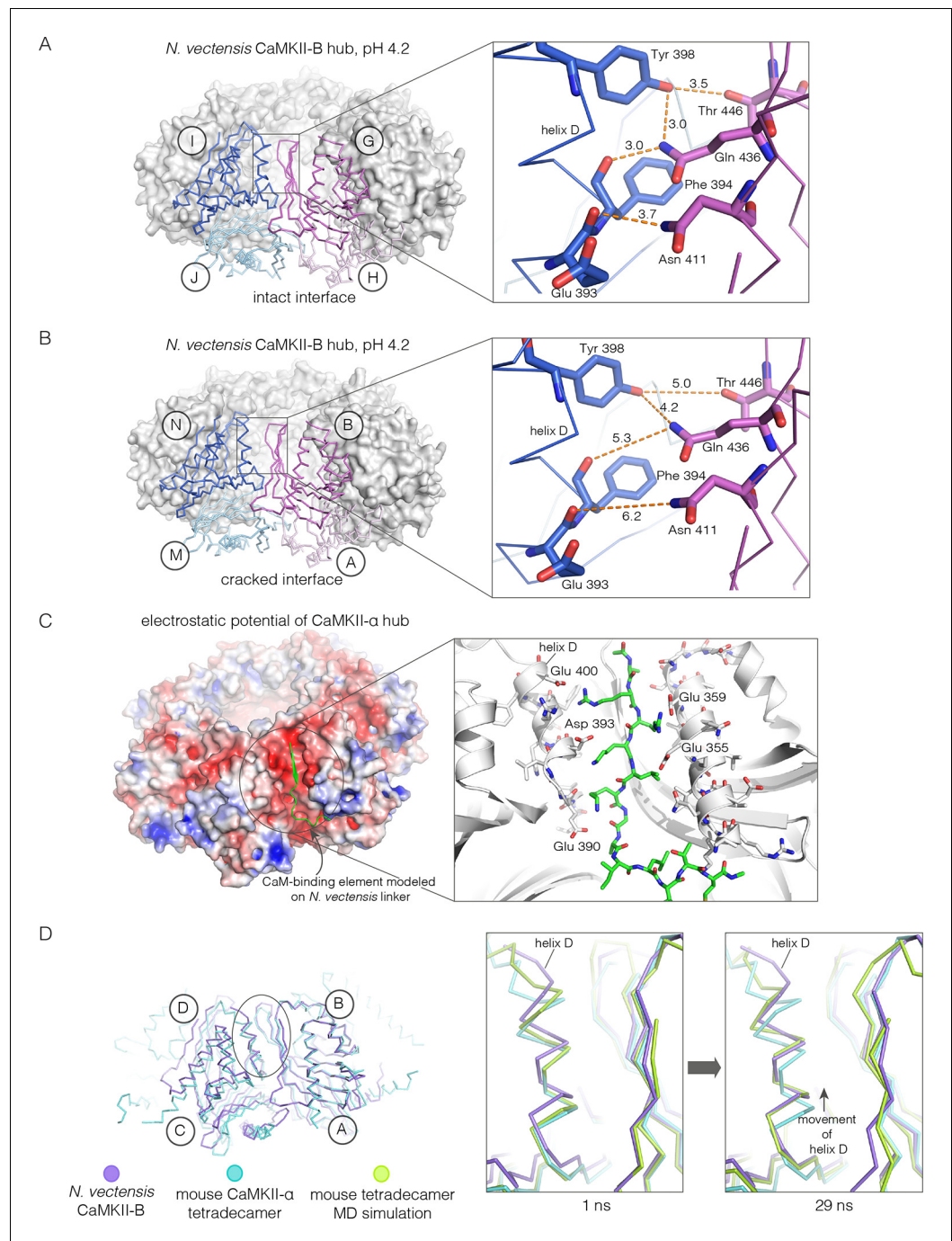


Figure 7. Analysis of the ring-opened *N. vectensis* CaMKII-B hub (pH 4.2) and its implications for docking of the CaM-binding element. **(A)** Interfacial hydrogen-bonding interactions at an intact interface in the *N. vectensis* CaMKII-B hub. **(B)** As in **(A)**, but for one of the cracked interfaces. Hydrogen-bonding interactions are disrupted at this interface. **(C)** Modeling of the RRCLK motif of the CaM-binding element docked onto a hub interface in the tetradecameric mouse CaMKII- α hub (PDB code: 1HKX), based on the *N. vectensis* CaMKII-B hub structure. The surface electrostatic potential of the CaMKII- α hub, calculated using the Adaptive Poisson-Boltzmann Solver (APBS) in PyMOL, is shown, with red and blue representing negative and positive electrostatic potential, respectively. The expanded view shows interactions between the modeled CaM-binding element and residues in the hub. **(D)** Left, structural superposition of the closed-ring tetradecameric mouse CaMKII- α hub (PDB code: 1HKX) on the ring-opened *N. vectensis* CaMKII-B hub. The structures were aligned using subunit B. Note that the disposition of helix D is different at the two interfaces (circled). The expanded views show instantaneous structures

Figure 7 continued on next page

Figure 7 continued

(at 1 ns and 29 ns) from a molecular dynamics trajectory of the mouse hub, with the modeled CaM-binding element. Note that helix D in the simulation moves from its initial position to one that is closer to the position of this helix in the ring-opened *N. vectensis* structure.

DOI: [10.7554/eLife.13405.016](https://doi.org/10.7554/eLife.13405.016)

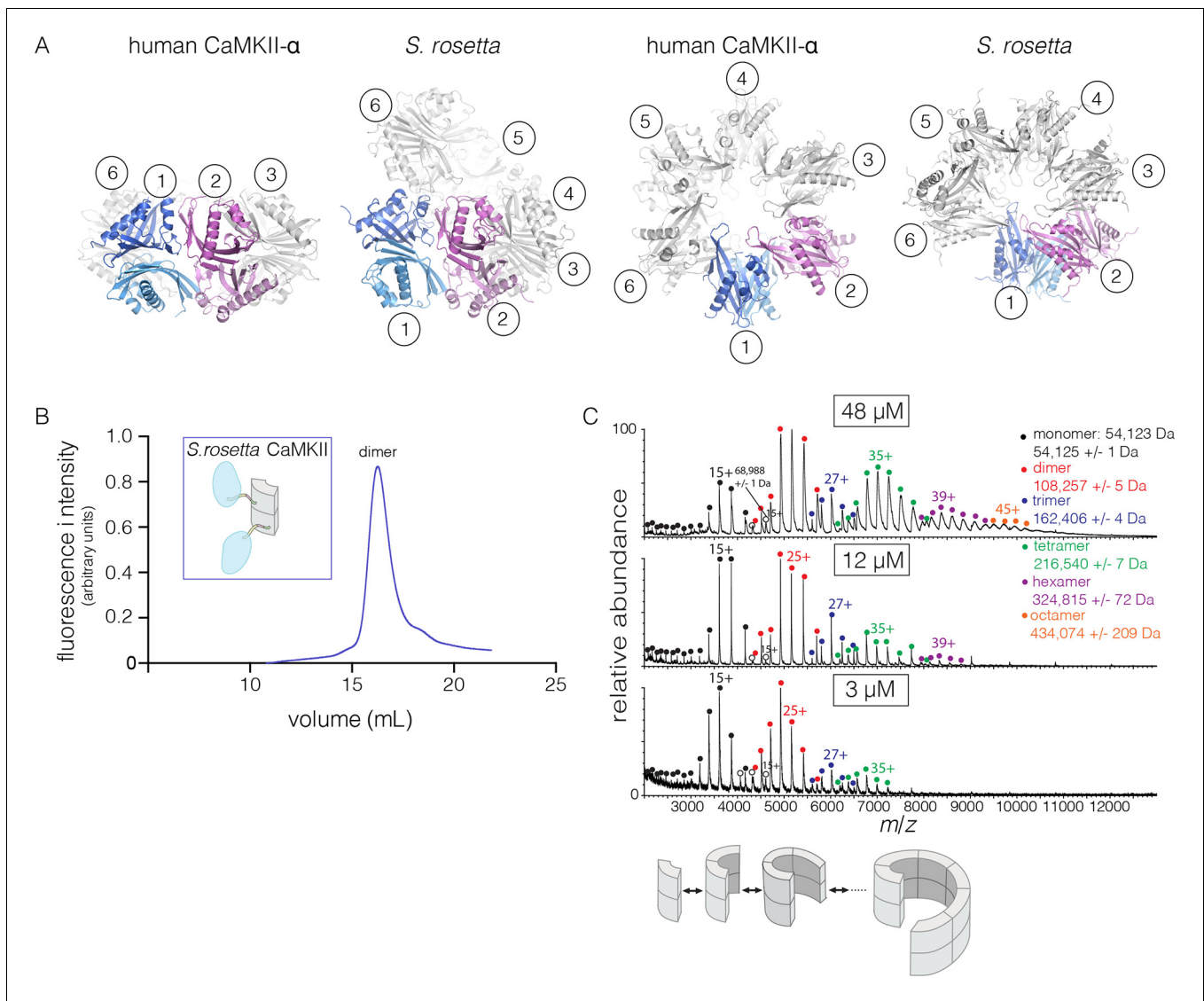


Figure 8. Structure and stoichiometry of the *S. rosetta* CaMKII. (A) Structural comparison of the hub assemblies of human CaMKII- α and *S. rosetta* CaMKII. Two views are shown for comparison and the six dimeric units are labeled 1–6. (B) Analytical gel filtration of *S. rosetta* CaMKII holoenzyme (blue) shows one predominant peak, corresponding to a dimeric species, as estimated from calibration data (see **Figure 4—figure supplement 4**). (C) Native electrospray-ionization mass spectrometry (ESI-MS) for the *S. rosetta* CaMKII holoenzyme at different concentrations. The proportion of higher order oligomeric species increases with increasing concentration, with an even number of subunits in each major species.

DOI: [10.7554/eLife.13405.017](https://doi.org/10.7554/eLife.13405.017)

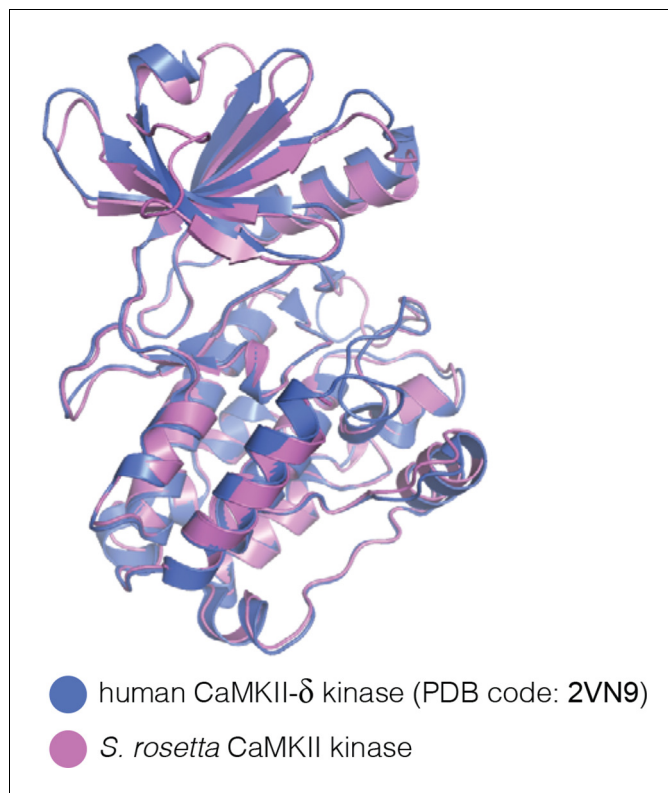


Figure 8—figure supplement 1. (A) Structural superposition of the autoinhibited kinase domain from *S. rosetta* CaMKII on the autoinhibited human CaMKII- δ kinase domain (PDB code: 2VN9).

DOI: [10.7554/eLife.13405.018](https://doi.org/10.7554/eLife.13405.018)

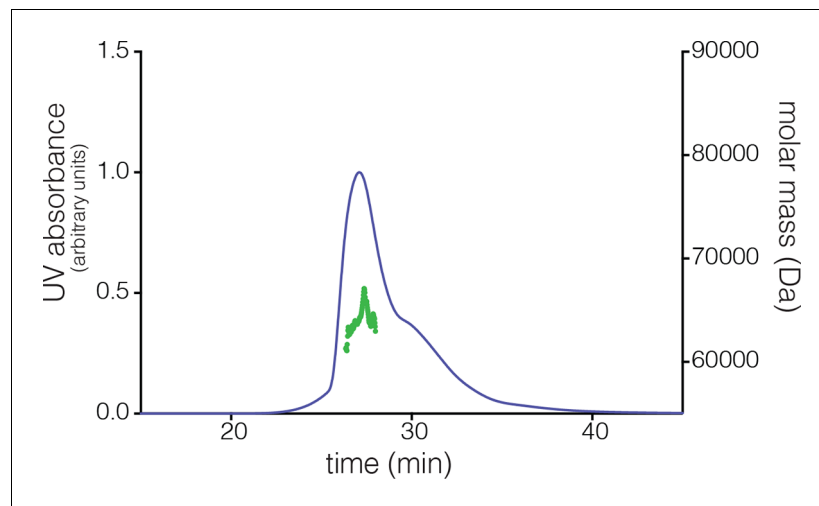


Figure 8—figure supplement 2. Multi-angle light scattering (MALS) analysis at a concentration of $\sim 200 \mu\text{M}$ reveals the existence of tetramers in *S. rosetta* CaMKII hub.

DOI: [10.7554/eLife.13405.019](https://doi.org/10.7554/eLife.13405.019)

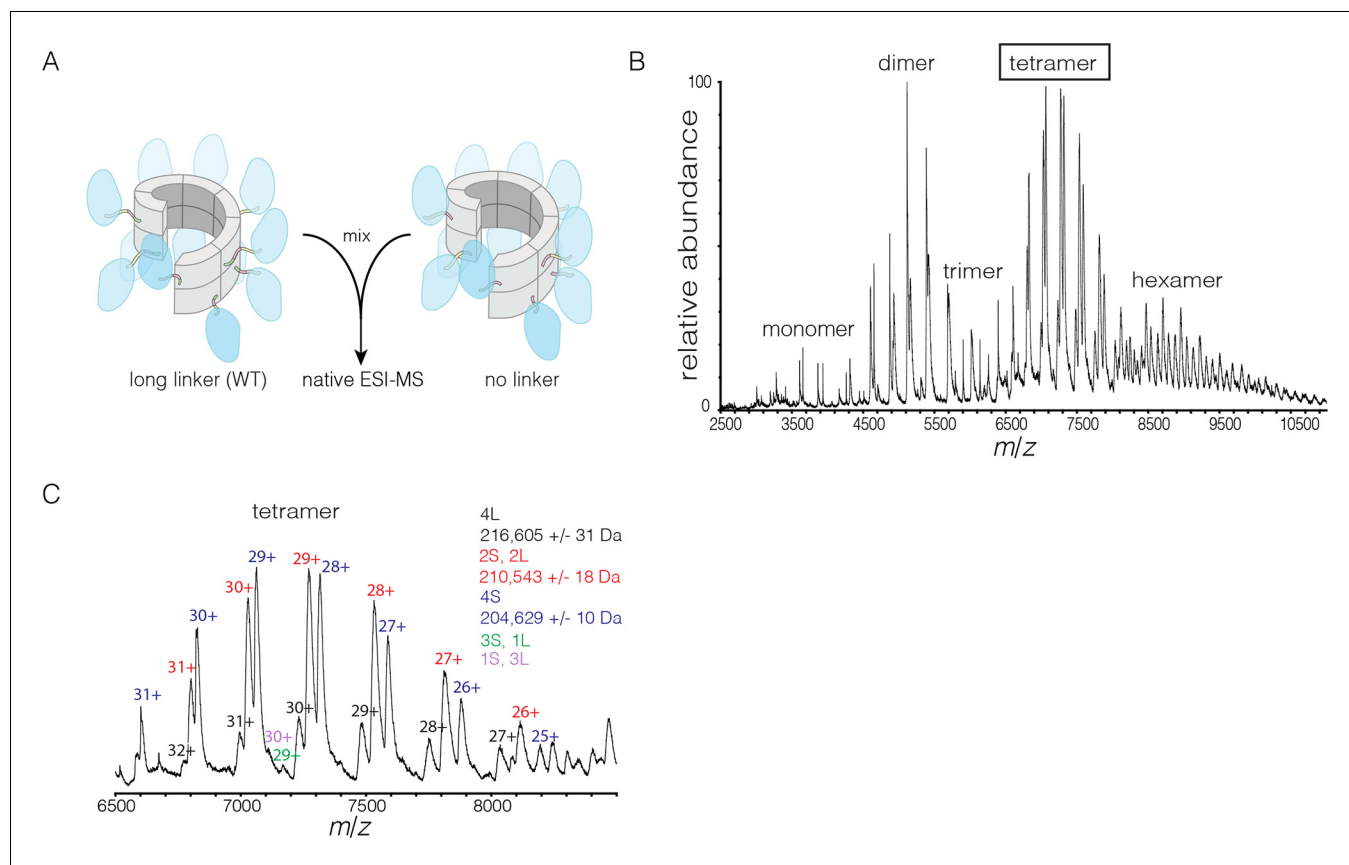


Figure 9. Subunit exchange in *S. rosetta* CaMKII monitored by ESI-MS. **(A)** Setup of the subunit exchange experiment for *S. rosetta* CaMKII. Wild-type CaMKII is mixed with a shorter version in which the linker is deleted, followed by mass spectrometric analysis. **(B)** Mass spectrum showing a mixture of multiple oligomeric species, ranging from monomer to hexamer. **(C)** Expansion of the mass spectrum in the region of the intact tetramer shows the existence of even numbers of long and short species. This indicates that subunit exchange in *S. rosetta* CaMKII occurs predominantly through the exchange of dimer units. 1L, 2L, 3L and 4L refer to CaMKII assemblies with one, two, three or four long (wild-type) subunits, respectively. Likewise, 1S, 2S, 3S and 4S refer to the corresponding numbers of short (no linker) subunits.

DOI: [10.7554/eLife.13405.020](https://doi.org/10.7554/eLife.13405.020)

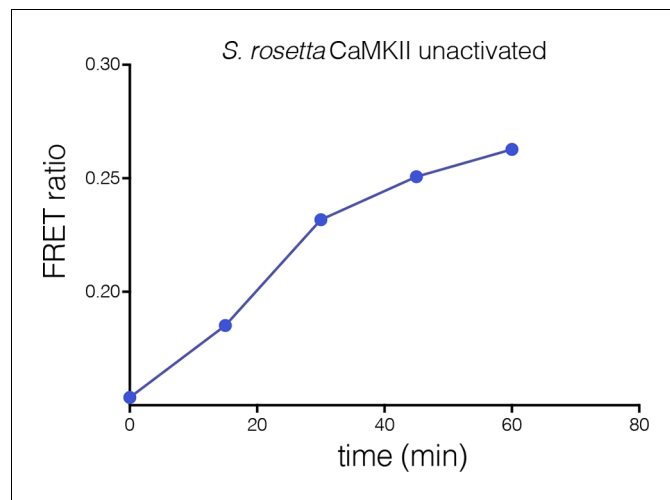


Figure 9—figure supplement 1. Spontaneous subunit exchange in *S. rosetta* CaMKII without activation. Increase in the FRET ratio is graphed as a function of time, exhibiting spontaneous subunit exchange upon mixing donor and acceptor-labeled proteins.

DOI: [10.7554/eLife.13405.021](https://doi.org/10.7554/eLife.13405.021)

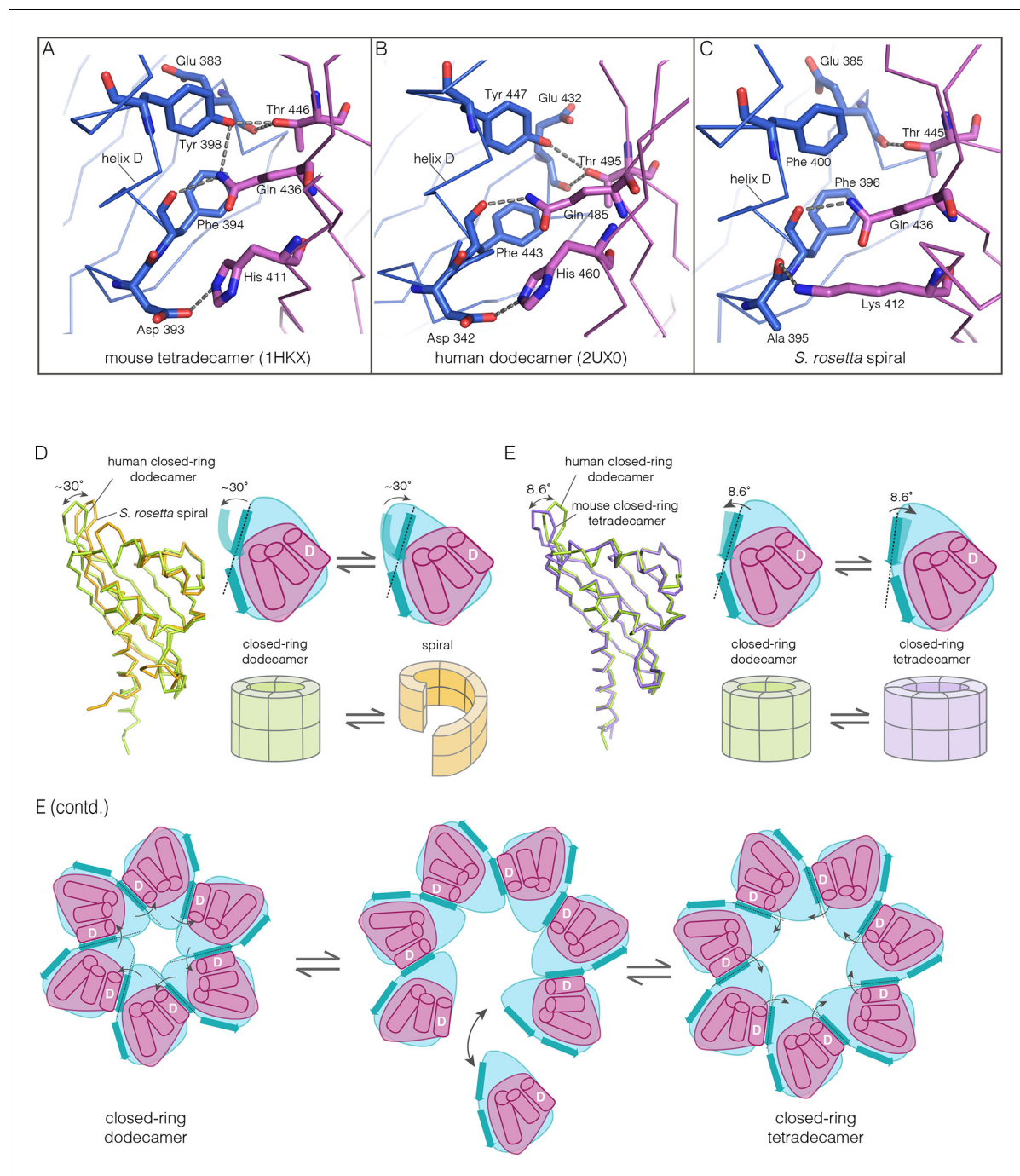


Figure 10. How the CaMKII hub accommodates assemblies with variable stoichiometry. (A–C) Comparison of interfacial interactions at the interface between vertical dimers in the mouse tetradecameric hub (PDB code: 1HKX), human dodecameric hub (PDB Code: 2UX0) and the *S. rosetta* hub respectively. (D) Structural comparison between a subunit of the *S. rosetta* spiral hub and a human dodecameric hub. The schematic diagram represents a hub domain in terms of two layers, one formed by the β -sheet and one by the α -helices. The conformational change in the hub in different assemblies corresponds to a change in the twist of the β -sheet. (E) Structural comparison of tetradecameric and dodecameric closed-ring hubs. Changes in the curvature of the β -sheet allow interfacial packing between adjacent subunits to be maintained in each case. The schematic illustration shows how a change in curvature of the β -sheet explains the transition from the dodecameric to the tetradecameric closed-ring forms, preserving the interfacial interactions.

DOI: [10.7554/eLife.13405.022](https://doi.org/10.7554/eLife.13405.022)

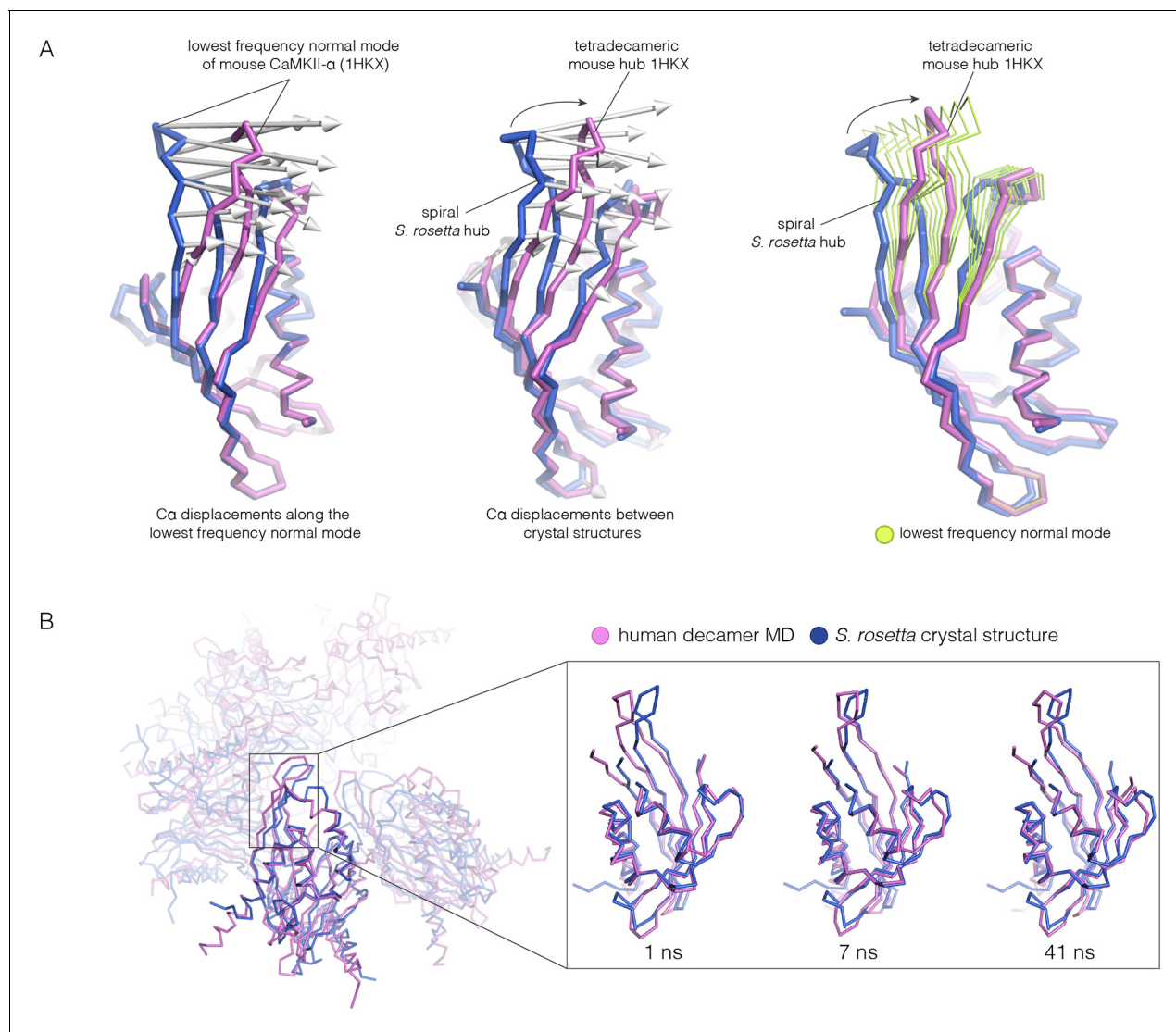


Figure 11. Normal mode calculation and molecular dynamics simulations for the mouse and human hub respectively. **(A)** Movement of the mouse CaMKII- α hub (PDB code: 1HKX) along the lowest-frequency internal normal mode recapitulates the structural differences in the *S. rosetta* hub. Normal modes were calculated using a vertical dimer from the mouse CaMKII- α hub, using an elastic network model (Suhre and Sanejouand, 2004). In the diagram on the left, displacement vectors corresponding to the lowest-frequency internal normal mode are shown by arrows. The structures shown in magenta and blue correspond to excursions of the mouse hub along this mode. In the middle, the structures of the mouse hub and the *S. rosetta* hub are compared, and the arrows show the displacement vectors between the two structures. The diagram on the right shows the structures of the mouse hub and the *S. rosetta* hub, and excursions of the mouse hub along the lowest-frequency internal normal mode (green). Note that the normal mode, calculated without reference to the *S. rosetta* structure, captures the essential features of the structural difference between the mouse and *S. rosetta* hub. **(B)** Comparison of the *S. rosetta* hub structure to instantaneous structures from a molecular dynamics trajectory for a decameric human hub assembly (the open decameric assembly is generated by removing a vertical dimer from the dodecameric hub ring; PDB code: 2UX0). Helices A to D in the *S. rosetta* hub are aligned to the corresponding helices in the instantaneous simulated structures. Three instantaneous structures from the trajectory, at 1, 7 and 41 ns, are shown. Note that the strands of the β -sheet in structures at 7 and 41 ns are closely aligned with the *S. rosetta* structure. DOI: 10.7554/eLife.13405.023

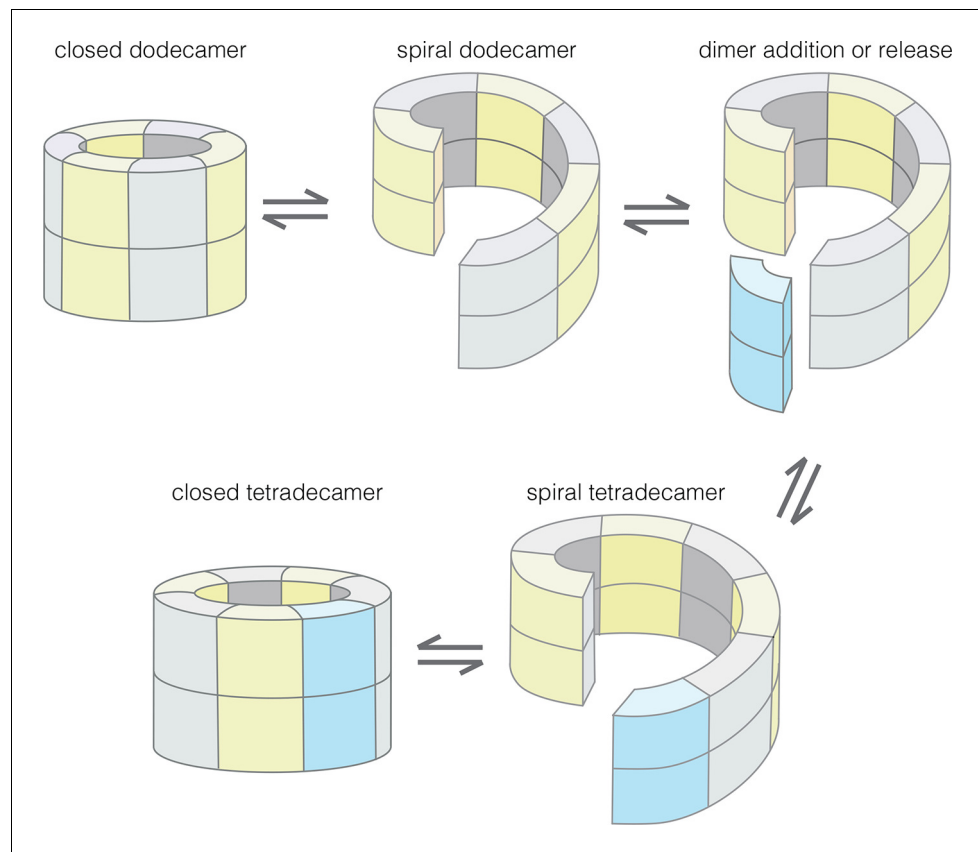


Figure 12. Model for the interconversion of dodecameric and tetradecameric assemblies by the CaMKII hub domain. This could potentially support an efficient subunit exchange mechanism that does not require complete disassembly and reassembly.

DOI: [10.7554/eLife.13405.024](https://doi.org/10.7554/eLife.13405.024)